Quantifying Disrupted Outer Retinal-Subretinal Layer in SD-OCT Images in Choroidal Neovascularization

Li Zhang,[1] Milan Sonka,[1,2] James C. Folk,[2] Stephen R. Russell,[2,3] and Michael D. Abràmoff[1–6]

[1]Department of Electrical and Computer Engineering, University of Iowa, Iowa City, Iowa, United States
[2]Department of Ophthalmology and Visual Sciences, University of Iowa Hospitals and Clinics, Iowa City, Iowa, United States
[3]Carver Family Center for Macular Degeneration, University of Iowa (Division of Institute for Vision Research), Iowa City, Iowa, United States
[4]Institute for Vision Research, University of Iowa, Iowa City, Iowa, United States
[5]Department of Veterans Affairs, Iowa City VA Medical Center, Iowa City, Iowa, United States
[6]Department of Biomedical Engineering, University of Iowa, Iowa City, Iowa, United States

Correspondence: Michael D. Abràmoff, Department of Ophthalmology and Visual Sciences, University of Iowa, 200 Hawkins Drive, Iowa City, IA 52242, USA;
michael-abramoff@uiowa.edu.

Submitted: August 13, 2013
Accepted: February 17, 2014

Citation: Zhang L, Sonka M, Folk JC, Russell SR, Abràmoff MD. Quantifying disrupted outer retinal-subretinal layer in SD-OCT images in choroidal neovascularization. *Invest Ophthalmol Vis Sci.* 2014;55:2329–2335. DOI:10.1167/iovs.13-13048

Purpose. We reported a fully automated method to identify and quantify the thickness of the outer retinal-subretinal (ORSR) layer from clinical spectral-domain optical coherence tomography (SD-OCT) scans of choroidal neovascularization (CNV) due to exudative age-related macular degeneration (eAMD).

Methods. A total of 23 subjects with CNV met eligibility. Volumetric SD-OCT scans of 23 eyes were obtained (Zeiss Cirrus, 200 × 200 × 1024 voxels). In a subset of eyes, scans were repeated. The OCT volumes were analyzed using our standard parameters and using a 3-dimensional (3D) graph-search approach with an adaptive cost function. A retinal specialist graded the segmentation as generally accurate, local segmentation inaccuracies, or failure. Reproducibility on repeat scans was analyzed using root mean square coefficient of variation (RMS CV) of the average ORSR thickness.

Results. Using a standard segmentation approach, 1/23 OCT segmentations was graded generally accurate and 22/23 were failure(s). With the adaptive method 21/23 segmentations were graded generally accurate; 2/23 were local segmentation inaccuracies and none was a failure. The intermethod quality of segmentation was significantly different ($P << 0.001$). The average ORSR thickness measured on CNV patients (78.0 μm; 95% confidence interval [CI], 72.5–83.4 μm) is significantly larger ($P << 0.001$) than normal average ORSR layer thickness (51.5 ± 3.3 μm). The RMS CV was 8.1%.

Conclusions. We have developed a fully automated 3D method for segmenting the ORSR layer in SD-OCT of patients with CNV from eAMD. Our method can quantify the ORSR layer thickness in the presence of fluid, which has the potential to augment management accuracy and efficiency of anti-VEGF treatment.

Keywords: retina, AMD, choroidal neovascularization, imaging, OCT

Approximately 10% of patients with age-related macular degeneration (AMD) have the exudative form of this disease.[1] Exudative AMD (eAMD) typically includes overt evidence of choroidal neovascularization (CNV), manifesting as retinal pigment epithelial detachment, subretinal and intraretinal cysts and fluid, retinal pigment epithelial tears, fibrovascular disciform scarring, and vitreous hemorrhage.[2] Recently, anti-VEGF agents have become the mainstay of treatment for CNV[3] in eAMD. In addition to visual acuity as a functional measurement, retinal thickening, location, and amount of intra- and subretinal fluid as imaged by optical coherence tomography (OCT) have become the principal milestones in the management of CNV with anti-VEGF agents.[4] Therefore, accurately and automatically segmenting the retinal structures in CNV is of great interest. Such a method has the potential to increase management accuracy and efficiency. However, CNV-associated retinal layer distortion that results from intra- and sub-retinal fluid accumulation makes accurate segmentation more challenging than in normal subjects or patients with atrophic diseases, such as glaucoma.[5] Fluid-associated abnormalities (Fig. 1) have been segmented using manual or semi-manual approaches,[6,7] but these methods are time-consuming, and suffer from intra- and interobserver variability. Previously, our group has developed the Iowa Reference Algorithms, an environment for fully automated 3-dimensional (3D) segmentation of retinal layer structures,[8] and also reported methods for detecting fluid-filled abnormalities in 2-dimensinal (2D) OCT projection images and in 3D volumes.[9,10] To enhance the robustness when segmenting intraretinal surfaces in normal subjects, these algorithms employ a strong distance constraint between myoid inner segment–ellipsoid inner segment (myoid IS–ellipsoid IS) and Bruch's membrane (BM). The increased thickness of the subretinal layers typical for CNV violates such distance constraints and may lead to segmentation errors. The present approach solves this problem by employing an adaptive cost function that is modulated based on the detection and OCT image properties describing the local structural abnormalities,

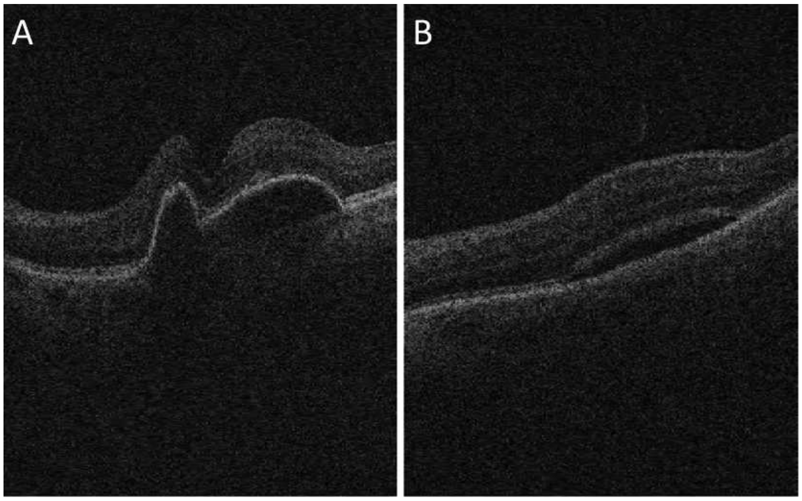

Figure 1. Exudative AMD in SD-OCT. (**A**) Pigment epithelial detachment. (**B**) Subretinal fluid.

and augments the distance constraints. We report a fully automated 3D method for segmenting the outer retinal-subretinal (ORSR) layer in spectral-domain OCT (SD-OCT) of patients with CNV and quantifying the ORSR layer thickness in the disrupted outer retina.

METHODS

Subject and Data Collection

We studied 23 patients, with an average age of 80.4 years (95% confidence interval [CI], 77.7–83.0 years); 39.1% (9 of 23) male, with clinically significant CNV underwent SD-OCT imaging (Zeiss Cirrus; Carl Zeiss Meditec, Inc., Dublin, CA). A total of 23 independent macula-centered volumetric scans was obtained from 23 eyes of these patients at the University of Iowa. Each volume was 200 × 200 × 1024 voxels (width of B-scan × number of B-scans × depth of B-scan), corresponding to physical dimensions of $6.0 \times 6.0 \times 2.0$ mm^3, and voxel size was $30.0 \times 30.0 \times 2.0$ µm^3. In 11 eyes from 11 subjects, repeat scans were obtained. Written informed consent was obtained from all subjects. The collection and analysis of image data were approved by Institutional Review Board of the University of Iowa, and adhered to the tenets of the Declaration of Helsinki.

Initial Segmentation

To reduce effects of and artifacts associated with retinal OCT imaging, and achieve successful retinal segmentation, the developed image analysis approach consisted of four subsequent stages. First, an initial segmentation was employed to detect ORSR layer using our previously reported 3D graph-based multilayer segmentation approach[11] (Figs. 2A, 2B). The initial segmentation provided approximate depth of the ORSR layer in the SD-OCT image. As expected, due to the shape complexity, and random distribution of subretinal fluids and pigment epithelial detachments, segmentation errors were present at this stage (Figs. 2C, 2D).

Fluid-Associated Abnormalities Detection

As discussed above, the varying shapes of ORSR layer resulting from the abnormalities increase the likelihood of incorrect segmentation. Stages 2 and 3 were used to locate the abnormal regions. By comparing textural properties of initially-segmented layers in AMD scans with an average texture of those layers in normal scans, a 2D "footprint" was computed in stage 2, identifying the locations of abnormal regions in the X-Y plane (Fig. 3).[9] In stage three, we applied a supervised voxel classification method to detect fluid-filled abnormalities in 3D. The inputs of this classification method, including structural, positional, and textural features, were derived from the original 3D volume data, 2D footprint images, and the initial segmentation. The structural and textural features described the local and regional image information, while positional features described the distance of individual layers from the initial segmentation. A k-nearest neighbor (kNN) classifier was chosen to classify OCT image voxels and evaluate in a leave-one-out fashion. A 3D probability map was calculated by determining the probability whether a voxel was located inside a fluid-filled region (Figs. 4A, 4B).[10]

ORSR Segmentation

In stage four, intensity gradient images were used to form the initial cost functions for a graph-search method to identify a full set of ORSR using a multi-scale graph-search method (Lee K, et al. *IOVS* 2010;51:ARVO E-Abstract 1767 and Ref. 12). As shown in Figure 4C, the bright line corresponding to Bruch's membrane (green line) was defined as the outer boundary of ORSR. The surface that corresponds to the transition between the myoid and ellipsoid inner segment (yellow line) was defined as the inner boundary of our outer retina segmentation.[13] For every node in the graph, the corresponding likelihood value on the 3D probability map was used as a weighting value to modify the initial cost function. Distance constraints were modified in response to the 3D probability map. For each A-scan, a higher probability value contributed to utilizing a larger distance constraint. Subsequently, the surfaces (myoid IS–ellipsoid IS and BM) are hierarchically segmented by identifying the minimum *s-t* cut in the employed geometric graphs, in which the weighted cost functions of vertical gradient transitions were utilized.

Validation of the ORSR Segmentation

After ORSR layer segmentation, the local ORSR thickness, defined as the Euclidian distance between myoid IS–ellipsoid IS and BM, was calculated along each A-scan, which is the summation of RPE thickness, outer segment length (OSL) ellipsoid inner segments,[14] and the height of any fluid-filled

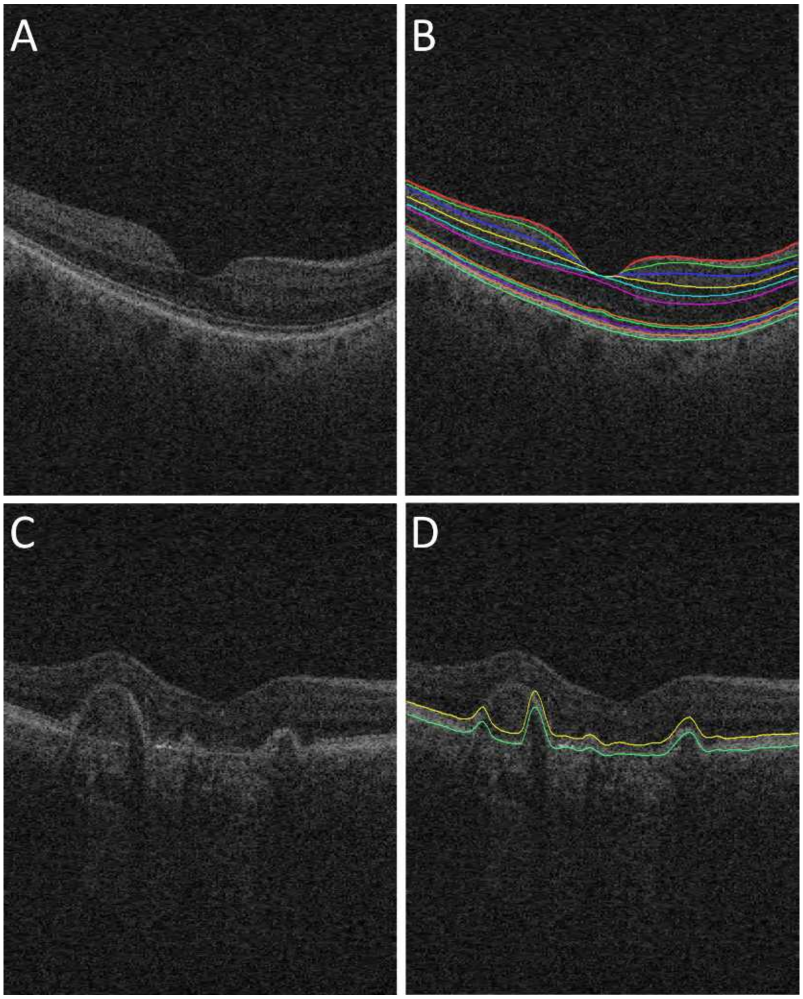

Figure 2. Retinal surfaces segmentation. (**A**) Original B-scan of 3D SD-OCT image from a normal subject. (**B**) Eleven retinal surfaces segmentation for the normal subject.[11] (**C**) Original B-scan of SD-OCT image from an exudative AMD patient. (**D**) Initial segmentation of ORSR surfaces of the exudative AMD patient, showing incorrect segmentation (*yellow surface*: myoid IS–ellipsoid IS; *green surface*: Bruch's membrane).

abnormalities. An ORSR layer thickness map for the 6 × 6 mm^2 macula-centered region as imaged by the SD-OCT then was created for all subjects (Fig. 5). A retinal specialist (MDA) who was blinded to the employed algorithm evaluated the segmentation performance of the original and new methods using a manual segmentation/review tool. Totals of 23 surface segmentation results of the present method and 23 results of the original method were mixed together in a random order. One original B-scan and the same B-scan with segmented surfaces depicted as layer boundaries always were displayed

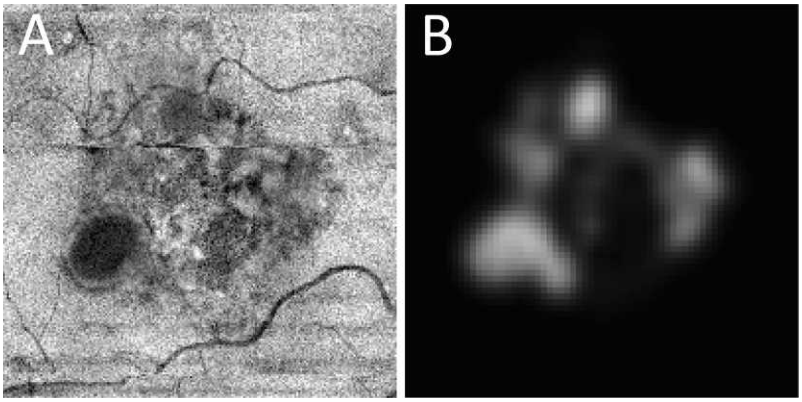

Figure 3. (**A**) ORSR projection image. (**B**) "Footprint" image of the fluid-filled abnormalities detected in the subretinal space.

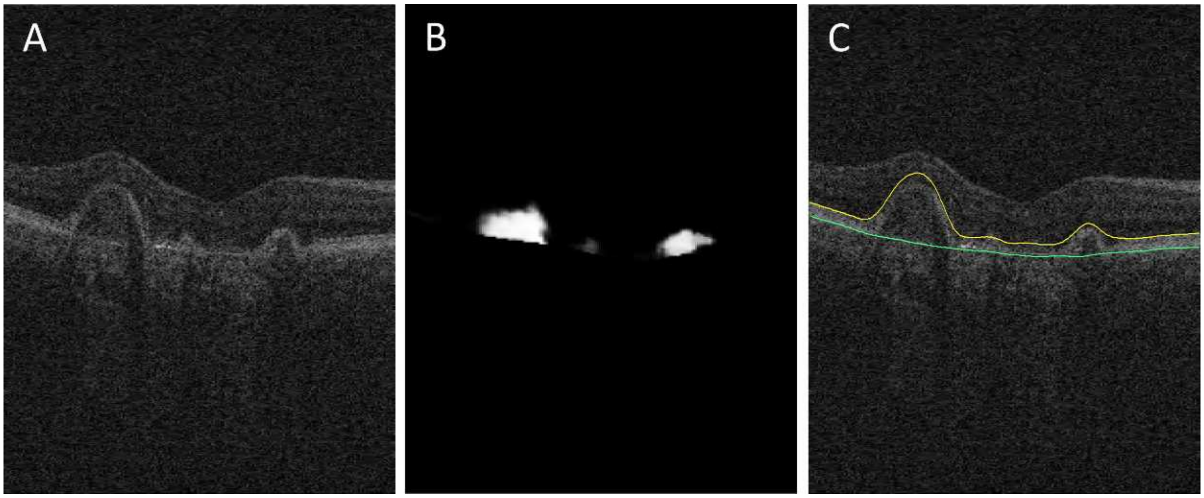

Figure 4. (**A**) Original B-scan. (**B**) Detection result of fluid-filled regions—the output of 3D voxel classification. (**C**) Surfaces segmentation result of ORSR layer: Bruch's membrane (*green surface*), and the surface that corresponds to the transition between the myoid IS–ellipsoid IS (*yellow surface*).

simultaneously to provide original unprocessed image to the expert observer. For each SD-OCT image data, the expert graded the segmentation result based on its correctness using three performance levels: generally accurate, local segmentation inaccuracies, and failure. The grading results of the two methods were compared using Fisher's exact test. A P value of 0.05 was considered significant.

Reproducibility Assessment

To evaluate the reproducibility of the proposed computerized method in the 11 repeat images (Fig. 6), coefficients of variation (CV) of the average ORSR thickness were calculated from two independent automated analyses using the root mean square (RMS) approach and the CV across the repeat analyses was computed.

Layer Thickness Assessment

Once the performance of the new method was established by the above validation experiment, the average thicknesses of the ORSR layers were computed from the results of the new image segmentation analysis in all 23 datasets—no datasets were excluded from the analysis and no segmentations were edited manually. The average thickness was reported in micrometers, 95% CIs were determined, and the obtained ORSR layer thickness compared to OCT specimens-established ORSR layer thickness in normal subjects.[15,16] The layer thicknesses of the two groups were statistically compared using t-tests with a P value of 0.05 considered significant.

RESULTS

With the original approach, 1/23 OCT datasets was "generally accurate," none was graded "local segmentation inaccuracies," and the remaining 22/23 were graded as "failure" (Fig. 7C). With the new approach, 21/23 segmentations were expert-graded as "generally accurate" (Fig. 7A); the remaining 2/23 were graded as "local segmentation inaccuracies" (Fig. 7B), and none was considered a "failure." This is a significant improvement (Fisher's exact test, $P << 0.001$, Fig. 8).

The reproducibility analysis tested the average ORSR thickness of repeat scans from the same patient and showed that the segmentation results of the present method are highly reproducible. As shown in Figure 9, RMS CV for ORSR was 8.1%.

Average ORSR thickness of the exudative AMD subjects in this study was 78.0 µm (95% CI, 72.5–83.4 µm) for the 6 × 6

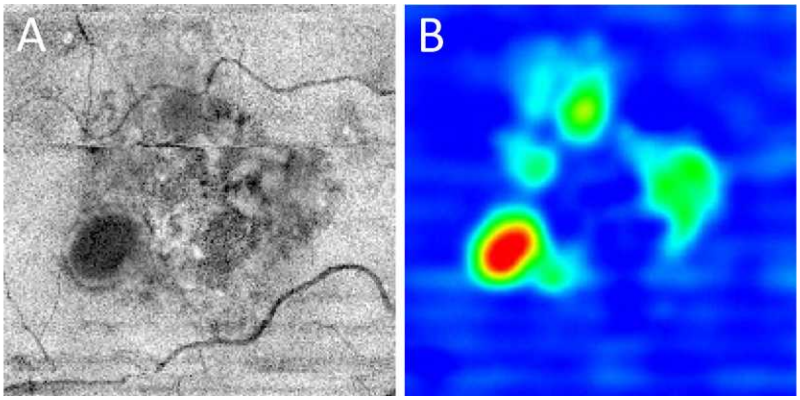

Figure 5. ORSR layer thickness maps. (**A**) ORSR projection image from the SD-OCT volume data. (**B**) An example thickness map of the proposed ORSR layer segmentation method, the average thickness on the analyzed 23 patients with CNV was 71.40 µm (maximum, 336.27 µm; minimum, 29.33 µm).

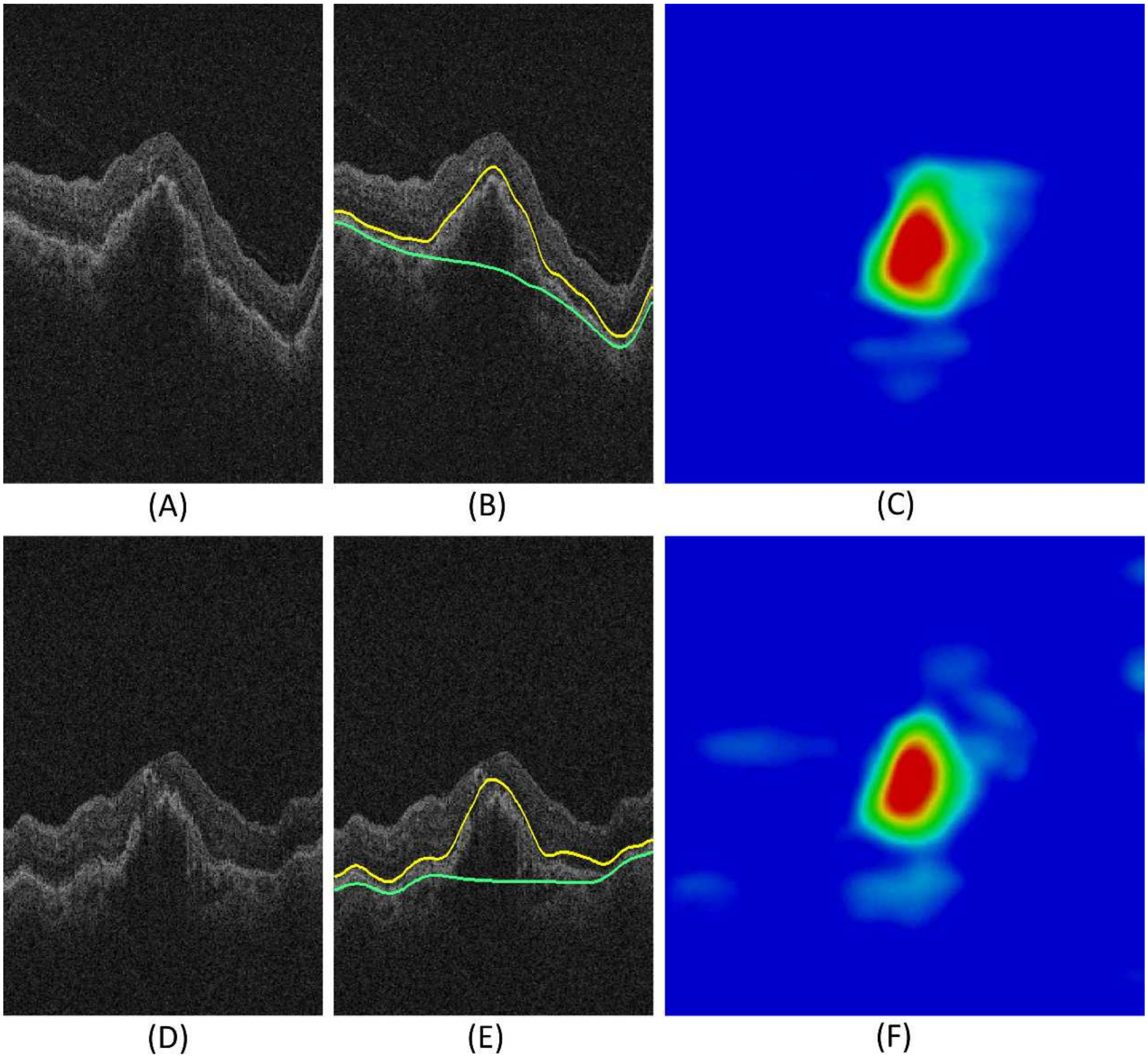

Figure 6. Reproducibility of ORSR layer segmentation. (**A–C**) First visit image data of an example subject. (**A**) Original slice. (**B**) ORSR segmentation (*yellow surface*: myoid IS–ellipsoid IS; *green surface*: Bruch's membrane). (**C**) Thickness map of the first visit image data. (**D–F**) Second visit image data of the same example subject. (**D**) Original slice. (**E**) ORSR segmentation (*yellow surface*: myoid IS–ellipsoid IS; *green surface*: Bruch's membrane). (**F**) Thickness map of the second visit image data.

mm^2 macula-centered region. Comparison with the finding on normal outer retinas in OCT specimens showed that average thickness (±SD) of the normal ORSR layer was 51.5 μm (±3.3 μm).[17] Not surprisingly, the ORSR thickness measured on CNV patients was significantly larger ($P << 0.001$) than the normal average ORSR layer thickness.

Discussion

The results showed that our new fully automated 3D method for segmenting the ORSR layer in SD-OCT of patients with CNV is able to successfully segment and subsequently quantify the ORSR layer thickness in the disrupted outer retina. Our new method successfully identified the ORSR layer affected with fluid-filled abnormalities in more than 90% (21 of 23) of cases in this data set. The segmentation inaccuracies that occurred in 2 of 23 datasets showed local inaccuracies that did not prevent the segmentation results from being used for quantitative analysis of the ORSR layer. The observed segmentation inaccuracies typically resulted from large solid tissue accumulation in the outer retina. In the OCT images, these solid tissues reduced the contrast around the ORSR, thus preventing the segmentation result from exactly locating the proper layer surface in the subretinal space. Simultaneously, the segmented surface of Bruch's membrane in these regions may be attracted by a higher contrast appearance of choroidal vessels as shown in Figure 7B. This dual effect may be the key reason for the observed local segmentation inaccuracies in the 2 identified datasets.

In our previously reported standard layer segmentation, fixed and strong constraints limited the distance between myoid IS–ellipsoid IS and BM, resulting in segmentation failure as shown in the expert evaluation. The reproducibility test showed the RMS CV of the standard layer segmentation to be 4.3%, which means similar segmentation failure may occur in the repeat scans of the patient. Compared to the standard layer segmentation with fixed and strong distance constraints, our new segmentation approach offers markedly better performance and improved the outcome in over 95% (22 of 23)

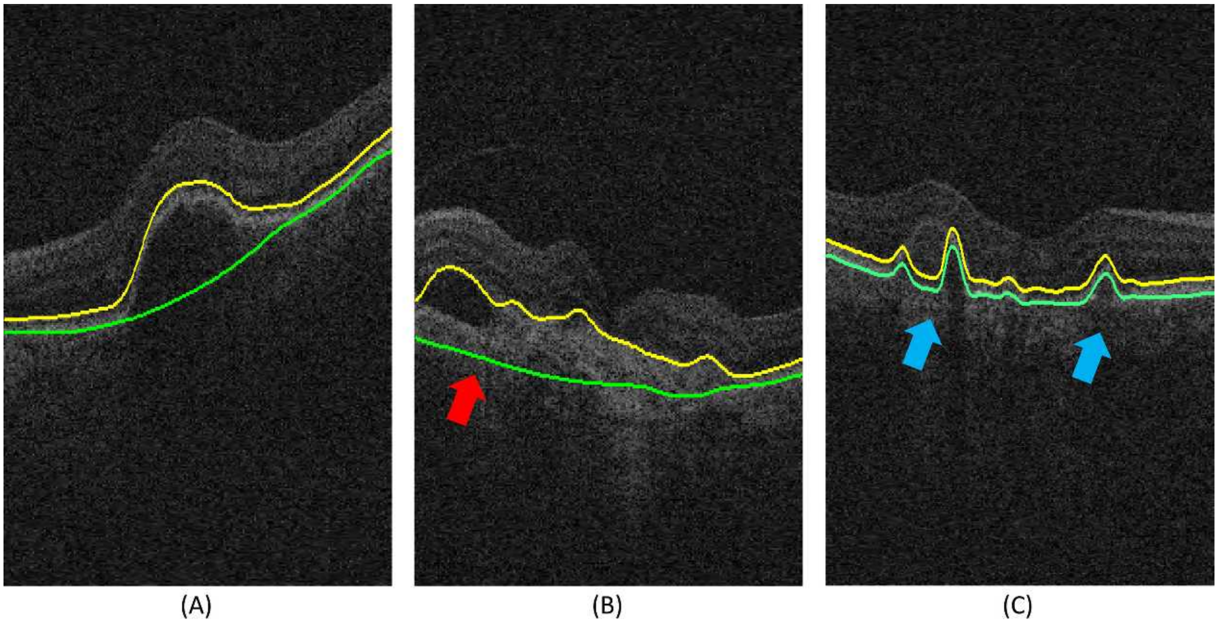

Figure 7. Examples of performance grading (*yellow surface*: myoid IS–ellipsoid IS; *green surface*: Bruch's membrane). (**A**) "Generally accurate" segmentation. (**B**) Segmentation that "includes local segmentation inaccuracies," marked by a *red arrow*. (**C**) "Failure," in proximity to the choroidal region, marked by *blue arrows*.

cases. Reproducibility of the new method also is high as shown by a RMS CV of 8.1%.

Due to the relatively low signal strength in standard clinically available SD-OCT data and random distribution of the fluid-filled abnormalities, automated segmentation of ORSR layer is challenging and surface detection results may become locally inaccurate within the subretinal space. However, as our study shows, these inaccuracies do not prevent the segmentation results to be used for quantitative analysis without manual editing.

To the best of our knowledge, this is the first 3D automated method capable of successfully segmenting the ORSR layer with a disrupted outer retina in exudative AMD scans. An example of 3D visualization of our new method's segmentation is provided in Figure 10. Accurate segmentation of the ORSR is essential for better automated quantification of subretinal and sub-RPE deposits, such as drusen, which are associated with the progression of AMD.

This study is not free of several limitations. First of all, the number of subjects was relatively small. Technically, the expert evaluation result showed the present method has improved the segmentation of outer retina affected by subretinal fluid and pigment epithelial detachment. However, the restricted size of the data set prevented us from learning clinically more important information, even though the proposed method provided more accurate segmentation results. We currently are pursuing a study with a larger population.

Second, we used clinically standard SD-OCT scanners with a center wavelength of 840 nm. The existence of fluid-filled

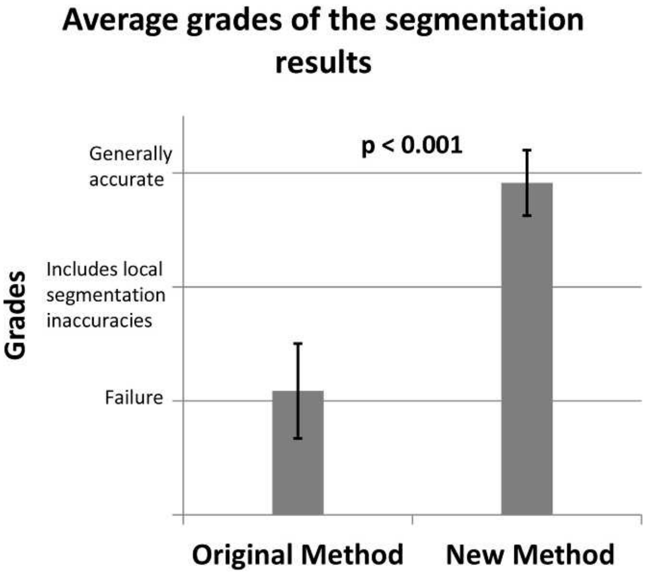

Figure 8. Performance comparison of the original and our new ORSR layer segmentation approaches based on expert evaluation.

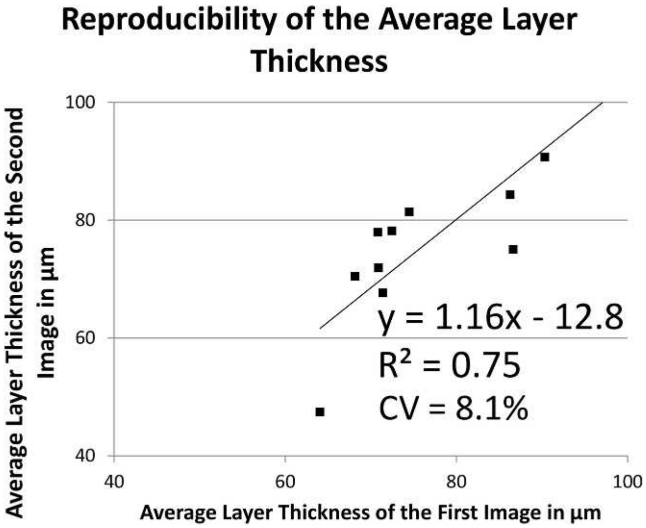

Figure 9. Reproducibility of automatically determined average ORSR layer thickness ($n = 11$).

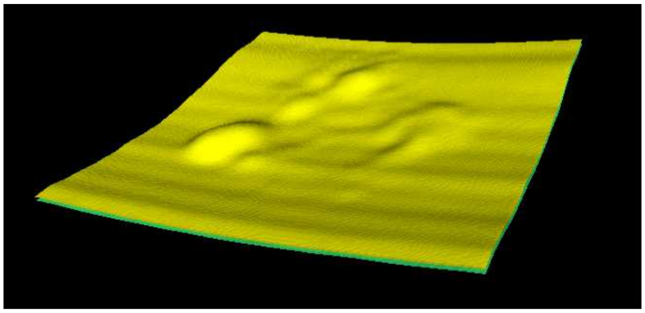

Figure 10. A 3D visualization of the ORSR layer obtained using the new segmentation approach in an OCT image of a CNV patient.

regions may resist the penetration of light, thus causing lower contrast around Bruch's membrane. Although the reproducibility analysis showed our proposed method performed robustly, enhanced depth imaging (EDI) and a longer center wavelength may improve further the accuracy of the layer segmentation.

In summary, we have developed a fully automated 3D method for segmenting the ORSR layer in SD-OCT of patients with exudative AMD, and quantifying the ORSR layer thickness in the occurrence of subretinal fluids and pigment epithelial detachments. The method outperformed our original layer segmentation and yielded robust segmentation outcomes as evaluated in the reproducibility studies. Our method has a potential to improve the diagnosis and management of patients with AMD and CNV.

Acknowledgments

Supported by Grants R01-EY017066 and R01-EY018853 (MDA, MS), and R01-EB004640 (MS).

Disclosure: **L. Zhang**, None; **M. Sonka**, P; **J.C. Folk**, None; **S.R. Russell**, None; **M.D. Abràmoff**, P

References

1. Ferris FL III, Fine SL, Hyman L. Age-related macular degeneration and blindness due to neovascular maculopathy. *Arch Ophthalmol*. 1984;102:1640–1642.
2. Bressler NM, Bressler SB, Fine SL. Age-related macular degeneration. *Surv Ophthalmol*. 1988;32:375–413.
3. Folk JC, Stone EM. Ranibizumab therapy for neovascular age-related macular degeneration. *N Engl J Med*. 2010;363:1648–1655.
4. Comparison of Age-Related Macular Degeneration Treatments Trials Research Group, Martin DF, Maguire MG, et al. Ranibizumab and bevacizumab for treatment of neovascular age-related macular degeneration: two-year results. *Ophthalmology*. 2012;119:1388–1398.
5. Garvin MK, Abramoff MD, Wu X, Russell SR, Burns TL, Sonka M. Automated 3-D intraretinal layer segmentation of macular spectral-domain optical coherence tomography images. *IEEE Trans Med Imaging*. 2009;28:1436–1447.
6. Ahlers C, Golbaz I, Einwallner E, et al. Identification of optical density ratios in subretinal fluid as a clinically relevant biomarker in exudative macular disease. *Invest Ophthalmol Vis Sci*. 2009;50:3417–3424.
7. Smretschnig E, Krebs I, Moussa S, Ansari-Shahrezaei S, Binder S. Cirrus OCT versus Spectralis OCT: differences in segmentation in fibrovascular pigment epithelial detachment. *Graefe's Arch Clin Exp Ophthalmol*. 2010;248:1693–1698.
8. Abramoff MD, Garvin M, Sonka M. Retinal imaging and image analysis. *IEEE Rev Biomed Eng*. 2010;169–208.
9. Quellec G, Lee K, Dolejsi M, Garvin MK, Abramoff MD, Sonka M. Three-dimensional analysis of retinal layer texture: identification of fluid-filled regions in SD-OCT of the macula. *IEEE Trans Med Imaging*. 2010;29:1321–1330.
10. Chen X, Niemeijer M, Zhang L, Lee K, Abramoff MD, Sonka M. Three-dimensional segmentation of fluid-associated abnormalities in retinal OCT: probability constrained graph-search-graph-cut. *IEEE Trans Med Imaging*. 2012;31:1521–1531.
11. Garvin MK, Abramoff MD, Kardon R, Russell SR, Wu X, Sonka M. Intraretinal layer segmentation of macular optical coherence tomography images using optimal 3-D graph search. *IEEE Trans Med Imaging*. 2008;27:1495–1505.
12. Lee K, Niemeijer M, Garvin MK, Kwon YH, Sonka M, Abramoff MD. Segmentation of the optic disc in 3-D OCT scans of the optic nerve head. *IEEE Trans Med Imaging*. 2010;29:159–168.
13. Spaide RF, Curcio CA. Anatomical correlates to the bands seen in the outer retina by optical coherence tomography: literature review and model. *Retina*. 2011;31:1609–1619.
14. Abramoff MD, Mullins RF, Lee K, et al. Human photoreceptor outer segments shorten during light adaptation. *Invest Ophthalmol Vis Sci*. 2013;54:3721–3728.
15. Huang DSE, Lin CP, Schuman JS, et al. Optical coherence tomography. *Science*. 1991;254:1178–1181.
16. Kiernan DF, Mieler WF, Hariprasad SM. Spectral-domain optical coherence tomography: a comparison of modern high-resolution retinal imaging systems. *Am J Ophthalmol*. 2010; 149:18–31.
17. Acton JH, Smith RT, Hood DC, Greenstein VC. Relationship between retinal layer thickness and the visual field in early age-related macular degeneration. *Invest Ophthalmol Vis Sci*. 2012;53:7618–7624.